
Spatio-Temporal Backpropagation for Training High-performance Spiking Neural Networks

Yujie Wu^{1†}, Lei Deng^{1†}, Guoqi Li^{1*}, Jun Zhu² and Luping Shi^{1*}

¹Center for Brain-Inspired Computing Research (CBICR),
Department of Precision Instrument,
Tsinghua University, 100084 Beijing, China

²State Key Lab of Intelligence Technology and System,
Tsinghua National Lab for Information Science and Technology,
Tsinghua University, 100084 Beijing, China

Abstract

Compared with artificial neural networks (ANNs), spiking neural networks (SNNs) are promising to explore the brain-like behaviors since the spikes could encode more spatio-temporal information. Although existing schemes including pre-training from ANN or direct training based on backpropagation (BP) make the supervised training of SNNs possible, these methods only exploit the networks' spatial domain information which leads to the performance bottleneck and requires many complicated training techniques. Another fundamental issue is that the spike activity is naturally non-differentiable which causes great difficulties in training SNNs. To this end, we build an iterative LIF model that is more friendly for gradient descent training. By simultaneously considering the layer-by-layer spatial domain (SD) and the timing-dependent temporal domain (TD) in the training phase, as well as an approximated derivative for the spike activity, we propose a spatio-temporal backpropagation (STBP) training framework without using any complicated skill. We design the corresponding fully connected and convolution architecture and evaluate our framework on the static MNIST and a custom object detection dataset, as well as the dynamic N-MNIST. Results show that our approach achieves the best accuracy compared with existing state-of-the-art algorithms. This work provides a new perspective to explore the high-performance SNNs for future brain-like computing paradigm with rich spatio-temporal dynamics.

1 Introduction

Deep neural networks (DNNs) have achieved outstanding performance in diverse areas [1–5], while it seems that the brain uses another network architecture, spiking neural networks (SNNs), to realize various complicated cognitive functions [6–8]. Compared with the existing DNNs, SNNs mainly have two superiorities: 1) the spike pattern flowing through SNNs fundamentally codes more spatio-temporal information, while most DNNs lack timing dynamics, especially the widely used feedfor-

[†]The authors contribute equally.

^{*}Corresponding: lpshi@tsinghua.edu.cn, liguoqi@tsinghua.edu.cn

ward DNNs; and 2) event-driven paradigm of SNNs can make it more hardware friendly, and be adopted by many neuromorphic platforms [9–14].

However, it remains challenging in training SNNs because of the quite complicated dynamics and non-differentiable nature of the spike activity. In summary, there exist three kinds of training methods for SNNs: 1) unsupervised learning; 2) indirect supervised learning; 3) direct supervised learning. The first one originates from the biological synaptic plasticity for weight modification, such as spike timing dependent plasticity (STDP) [15–17]. Because it only considers the local neuronal activities, it is difficult to achieve high performance. The second one firstly trains an ANN, and then transforms it into its SNN version with the same network structure where the spiking rate of SNN neurons acts as the analog activity of ANN neurons [18–21]. This is not a bio-plausible way to explore the learning nature of SNNs. The most promising method to obtain high-performance training is the recent direct supervised learning based on the gradient descent theory with error backpropagation. However, such a method only considers the layer-by-layer spatial domain (SD) and ignores the dynamics in temporal domain (TD) [22, 23]. Therefore many complicated training skills are required to improve performance [19, 23, 24], such as fixed-amount-proportional reset, lateral inhibition, error normalization, weight/threshold regularization, etc. Thus, a more general dynamic model and learning framework on SNNs are highly required.

In this paper, we propose a novel supervised learning framework for SNNs which combines both the SD and TD in the training phase for the first time. Firstly, we build an iterative LIF model with SNNs dynamics but it is friendly for gradient descent training. Then we consider both the spatial direction and temporal direction during the error backpropagation procedure, i.e, spatio-temporal backpropagation (STBP), which significantly improves the network accuracy. Furthermore, we introduce an approximated derivative to address the non-differentiable issue of the spike activity. We test our SNNs framework by using the fully connected and convolution architecture on the static MNIST and a custom object detection dataset, as well as the dynamic N-MNIST. Many complicated training skills which are generally required by existing schemes, can be avoided due to the fact that our proposed method can make full use of STD information that captures the nature of SNNs. Experimental results show that our proposed method could achieve the best accuracy on either static or dynamic dataset, compared with existing state-of-the-art algorithms. The influence of TD dynamics and different methods for the derivative approximation are systematically analyzed. This work shall open a way to explore the high-performance SNNs for future brain-like computing paradigms with rich STD dynamics.

2 Method and Material

2.1 Iterative Leaky Integrate-and-Fire Model in Spiking Neural Networks

Compared with existing deep neural networks (DNNs), spiking neural networks (SNNs) fundamentally code more spatio-temporal information due to two facts that i) SNNs can also have deep architectures like DNNs, and ii) each neuron has its own neuronal dynamic properties. The former one grants SNNs rich spatial domain (SD) information while the later one offers SNNs the power of encoding temporal domain (TD) information. However, currently there is no unified framework that allows the effective training of SNNs just as implementing backpropagation (BP) in DNNs by considering the spatio-temporal dynamics. This has challenged the extensive use of SNNs in various applications. In this work, we will present a novel framework based on iterative leaky integrate-and-fire (LIF) model that enables us to apply spatio-temporal backpropagation (STBP) for training spiking neural networks.

It is known that LIF is the most widely applied model to describe the neuronal dynamics in SNNs, and it can be simply governed by

$$\tau \frac{du(t)}{dt} = -u(t) + I(t) \quad (1)$$

where $u(t)$ is the neuronal membrane potential at time t , τ is a time constant and $I(t)$ denotes the pre-synaptic input which is determined by the pre-neuronal activities or external injections and the synaptic weights. When the membrane potential u exceeds a given threshold V_{th} , the neuron

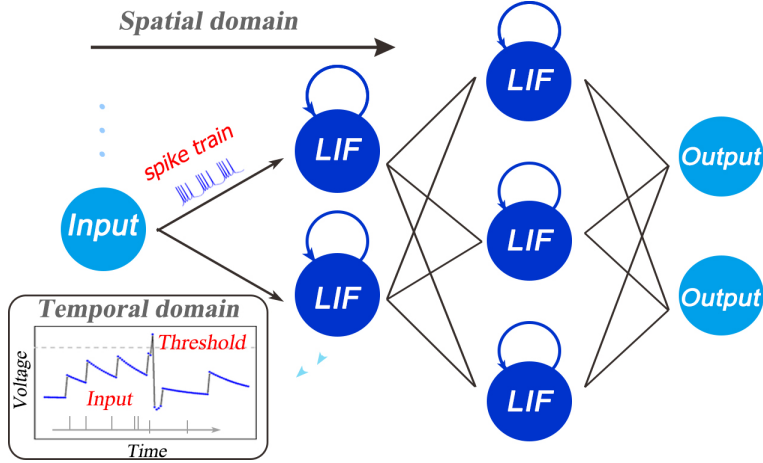


Figure 1: **Illustration of the spatio-temporal characteristic of SNNs.** Besides the layer-by-layer spatial dataflow like ANNs, SNNs are famous for the rich temporal dynamics and non-volatile potential integration. However, the existing training algorithms only consider either the spatial domain (SD) such as the supervised ones via backpropagation, or the temporal domain (TD) such as the unsupervised ones via timing-based plasticity, which causes the performance bottleneck. Therefore, how to build an learning framework making full use of the spatio-temporal domain (STD) is fundamentally required for high-performance SNNs that forms the main motivation of this work.

fires a spike and resets its potential to u_{reset} . As shown in Figure 1, the forward dataflow of the SNN propagates in the layer-by-layer SD like DNNs, and the self-feedback injection at each neuron node generates non-volatile integration in the TD. In this way, the whole SNN runs with complex STD dynamics and codes spatio-temporal information into the spike pattern. The existing training algorithms only consider either the SD such as the supervised ones via backpropagation, or the TD such as the unsupervised ones via timing-based plasticity, which causes the performance bottleneck. Therefore, how to build an learning framework making full use of the STD is fundamentally required for high-performance SNNs that forms the main motivation of this work.

However, obtaining the analytic solution of LIF model in (1) directly makes it inconvenient/obscure to train SNNs based on backpropagation (BP). This is because the whole network shall present complex dynamics in both SD and TD. To address this issue, the following event-driven iterative updating rule

$$u(t) = u(t_{i-1})e^{-\frac{t-t_{i-1}}{\tau}} + I(t) \quad (2)$$

can be well used to approximate the neuronal potential $u(t)$ in (1) based on the last spiking moment t_{i-1} and the pre-synaptic input $I(t)$. The membrane potential exponentially decays until the neuron receives pre-synaptic inputs, and a new update round will start once the neuron fires a spike. That is to say, the neuronal states are co-determined by the spatial accumulations of $I(t)$ and the leaky temporal memory of $u(t_{i-1})$.

As we know, the efficiency of error backpropagation for training DNNs greatly benefits from the iterative representation of gradient descent which yields the chain rule for layer-by-layer error propagation in the SD backward pass. This motivates us to propose a novel iterative LIF based SNN in which the iterations occur in both the SD and TD as follows:

$$x_i^{t+1,n} = \sum_{j=1}^{l(n-1)} w_{ij}^n o_j^{t+1,n-1} \quad (3)$$

$$u_i^{t+1,n} = u_i^{t,n} f(o_i^{t,n}) + x_i^{t+1,n} + b_i^n \quad (4)$$

$$o_i^{t+1,n} = g(u_i^{t+1,n}) \quad (5)$$

where

$$f(x) = \tau e^{-\frac{x}{\tau}} \quad (6)$$

$$g(x) = \begin{cases} 1, & x \geq V_{th} \\ 0, & x < V_{th} \end{cases} \quad (7)$$

In above formulas, the upper index t denotes the moment at time t , and n and $l(n)$ denote the n th layer and the number of neurons in the n th layer, respectively. w_{ij} is the synaptic weight from the j th neuron in pre-synaptic layer to the i th neuron in the post-synaptic layer, and $o_j \in \{0, 1\}$ is the neuronal output of the j th neuron where $o_j = 1$ denotes a spike activity and $o_j = 0$ denotes nothing occurs. x_i is a simplified representation of the pre-synaptic inputs of the i th neuron, similar to the I in the original LIF model. u_i is the neuronal membrane potential of the i th neuron and b_i is a bias parameter related the threshold V_{th} .

Actually, formulas (4)-(5) are also inspired from the LSTM model [25–27] by using a forget gate $f(\cdot)$ to control the TD memory and an output gate $g(\cdot)$ to fire a spike. The forget gate $f(\cdot)$ controls the leaky extent of the potential memory in the TD, the output gate $g(\cdot)$ generates a spike activity when it is activated. Specifically, for a small positive time constant τ , $f(\cdot)$ can be approximated as

$$f(o_i^{t,n}) \approx \begin{cases} \tau, & o_i^{t,n} = 0 \\ 0, & o_i^{t,n} = 1 \end{cases} \quad (8)$$

since $\tau e^{-\frac{1}{\tau}} \approx 0$. In this way, the original LIF model could be transformed to an iterative version where the recursive relationship in both the SD and TD is clearly describe, which is friendly for the following gradient descent training in the STD.

2.2 Spatio-Temporal Backpropagation Training

In order to present STBP training methodology, we define the following loss function L in which the mean square error for all samples under a given time windows T is to be minimized

$$L = \frac{1}{2S} \sum_{s=1}^S \left\| \mathbf{y}_s - \frac{1}{T} \sum_{t=1}^T \mathbf{o}_s^{t,N} \right\|_2^2 \quad (9)$$

where \mathbf{y}_s and \mathbf{o}_s denote the label vector of the s th training sample and the neuronal output vector of the last layer N , respectively.

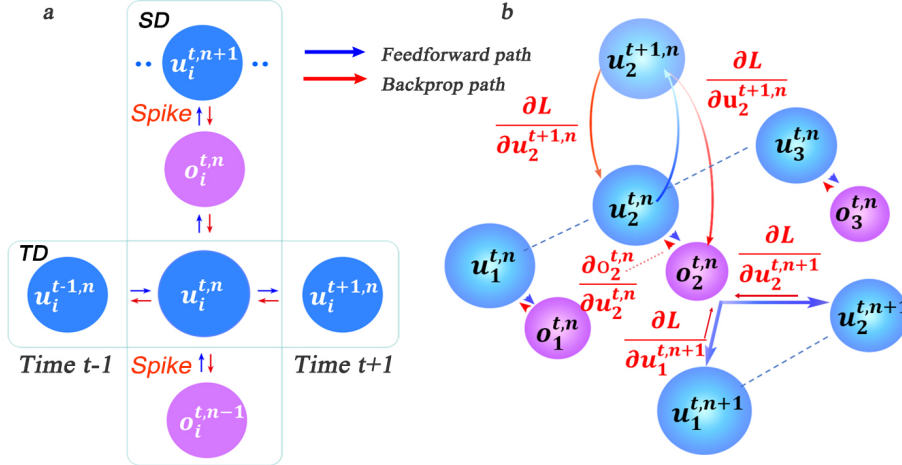


Figure 2: **Error propagation in the STD.** (a) At the single-neuron level, the vertical path and horizontal path represent the error propagation in the SD and TD, respectively. (b) Similar propagation occurs at the network level, where the error in the SD requires the multiply-accumulate operation like the feedforward computation.

By combining equations (3)-(9) together it can be seen that L is a function of \mathbf{W} and \mathbf{b} . Thus, to obtain the derivative of L with respect to \mathbf{W} and \mathbf{b} is required for the STBP algorithm based on

gradient descent. Assume that we have obtained derivative of $\frac{\partial L}{\partial o_i}$ and $\frac{\partial L}{\partial u_i}$ at each layer n at time t , which is an essential step to obtain the final $\frac{\partial L}{\partial \mathbf{W}}$ and $\frac{\partial L}{\partial \mathbf{b}}$. Figure 2 describes the error propagation (dependent on the derivation) in both the SD and TD at the single-neuron level (figure 2.a) and the network level (figure 2.b). At the single-neuron level, the propagation is decomposed into a vertical path of SD and a horizontal path of TD. The dataflow of error propagation in the SD is similar to the typical BP for DNNs, i.e. each neuron accumulates the weighted error signals from the upper layer and iteratively updates the parameters in different layers; while the dataflow in the TD shares the same neuronal states, which makes it quite complicated to directly obtain the analytical solution. To solve this problem, we use the proposed iterative LIF model to unfold the state space in both the SD and TD direction, thus the states in the TD at different time steps can be distinguished that enables the chain rule for iterative propagation. Similar idea can be found in the BPTT algorithm for training RNNs in [28].

Now, we discuss how to obtain the complete gradient descent based on the following four cases. Firstly, we denote that

$$\delta_i^{t,n} = \frac{\partial L}{\partial o_i^{t,n}} \quad (10)$$

Case 1: $t = T$ at the output layer $n = N$.

In this case, the derivative $\frac{\partial L}{\partial o_i^{T,N}}$ can be directly obtained since it depends on the loss function in Eq.(9) of the output layer. We could have

$$\frac{\partial L}{\partial o_i^{T,N}} = -\frac{1}{TS} \left(y_i - \frac{1}{T} \sum_{k=1}^T o_i^{k,N} \right). \quad (11)$$

The derivation with respect to $u_i^{T,N}$ is generated based on $o_i^{T,N}$

$$\frac{\partial L}{\partial u_i^{T,N}} = \frac{\partial L}{\partial o_i^{T,N}} \frac{\partial o_i^{T,N}}{\partial u_i^{T,N}} = \delta_i^{T,N} \frac{\partial o_i^{T,N}}{\partial u_i^{T,N}}. \quad (12)$$

Case 2: $t = T$ at the layers $n < N$.

In this case, the derivative $\frac{\partial L}{\partial o_i^{T,n}}$ iteratively depends on the error propagation in the SD at time T as the typical BP algorithm. We have

$$\frac{\partial L}{\partial o_i^{T,n}} = \sum_{j=1}^{l(n+1)} \delta_j^{T,n+1} \frac{\partial o_j^{T,n+1}}{\partial o_i^{T,n}} = \sum_{j=1}^{l(n+1)} \delta_j^{T,n+1} \frac{\partial g}{\partial u_i^{T,n}} w_{ji}. \quad (13)$$

Similarly, the derivative $\frac{\partial L}{\partial u_i^{T,n}}$ yields

$$\frac{\partial L}{\partial u_i^{T,n}} = \frac{\partial L}{\partial u_i^{T+1,n}} \frac{\partial u_i^{T+1,n}}{\partial u_i^{T,n}} = \frac{\partial L}{\partial u_i^{T+1,n}} f(o_i^{T+1,n}). \quad (14)$$

Case 3: $t < T$ at the output layer $n = N$.

In this case, the derivative $\frac{\partial L}{\partial o_i^{t,N}}$ depends on the error propagation in the TD direction. With the help of the proposed iterative LIF model in Eq.(3)-(5) by unfolding the state space in the TD, we acquire the required derivative based on the chain rule in the TD as follows

$$\frac{\partial L}{\partial o_i^{t,N}} = \delta_i^{t+1,N} \frac{\partial o_i^{t+1,N}}{\partial o_i^{t,N}} + \frac{\partial L}{\partial o_i^{t,N}} = \delta_i^{t+1,N} \frac{\partial g}{\partial u_i^{t+1,N}} u_i^{t,N} \frac{\partial f}{\partial o_j^{t,N}} + \frac{\partial L}{\partial o_i^{t,N}}, \quad (15)$$

$$\frac{\partial L}{\partial u_i^{t,N}} = \frac{\partial L}{\partial o_i^{t,N}} \frac{\partial o_i^{t,N}}{\partial u_i^{t,N}} = \delta_i^{t,N} \frac{\partial g}{\partial u_i^{t,N}}, \quad (16)$$

where $\frac{\partial L}{\partial o_i^{T,N}} = -\frac{1}{TS} \left(y_i - \frac{1}{T} \sum_{k=1}^T o_i^{k,N} \right)$ as in Eq.(11).

Case 4: $t < T$ at the layers $n < N$.

In this case, the derivative $\frac{\partial L}{\partial o_i^{t,n}}$ depends on the error propagation in both SD and TD. On one side, each neuron accumulates the weighted error signals from the upper layer in the SD like Case 2; on

the other side, each neuron also receives the propagated error from self-feedback dynamics in the TD by iteratively unfolding the state space based on the chain rule like Case 3. So we have

$$\frac{\partial L}{\partial o_i^{t,n}} = \sum_{j=1}^{l(n+1)} \delta_j^{t,n+1} \frac{\partial o_j^{t,n+1}}{\partial o_i^{t,n}} + \frac{\partial L}{\partial o_i^{t+1,n}} \frac{\partial o_i^{t+1,n}}{\partial o_i^{t,n}} \quad (17)$$

$$= \sum_{j=1}^{l(n+1)} \delta_j^{t,n+1} \frac{\partial g}{\partial u_i^{t,n}} w_{ji} + \delta_i^{t+1,n} \frac{\partial g}{\partial u_i^{t,n}} u_i^{t,n} \frac{\partial f}{\partial o_i^{t,n}}, \quad (18)$$

$$\frac{\partial L}{\partial u_i^{t,n}} = \frac{\partial L}{\partial o_i^{t,n}} \frac{\partial o_i^{t,n}}{\partial u_i^{t,n}} + \frac{\partial L}{\partial u_i^{t+1,n}} \frac{\partial u_i^{t+1,n}}{\partial u_i^{t,n}} \quad (19)$$

$$= \delta_i^{t,n} \frac{\partial g}{\partial u_i^{t,n}} + \frac{\partial L}{\partial u_i^{t+1,n}} f(o_i^{t+1,n}). \quad (20)$$

Based on the four cases, the error propagation procedure (depending on the above derivatives) is shown in Figure2. At the single-neuron level (Figure2.a), the propagation is decomposed into the vertical path of SD and the horizontal path of TD. At the network level (Figure2.b), the dataflow of error propagation in the SD is similar to the typical BP for DNNs, i.e. each neuron accumulates the weighted error signals from the upper layer and iteratively updates the parameters in different layers; and in the TD the neuronal states are unfolded iteratively in the timing direction that enables the chain-rule propagation. Finally, we obtain the derivatives with respect to \mathbf{W} and \mathbf{b} as follows

$$\frac{\partial L}{\partial \mathbf{b}^n} = \sum_{t=1}^T \frac{\partial L}{\partial \mathbf{u}^{t,n}} \frac{\partial \mathbf{u}^{t,n}}{\partial \mathbf{b}^n} = \sum_{t=1}^T \frac{\partial L}{\partial \mathbf{u}^{t,n}}, \quad (21)$$

$$\frac{\partial L}{\partial \mathbf{W}^n} = \sum_{t=1}^T \frac{\partial L}{\partial \mathbf{u}^{t,n}} \frac{\partial \mathbf{u}^{t,n}}{\partial \mathbf{W}^n} = \sum_{t=1}^T \frac{\partial L}{\partial \mathbf{u}^{t,n}} \mathbf{o}^{t,n-1T}, \quad (22)$$

where $\frac{\partial L}{\partial \mathbf{u}^{t,n}}$ can be obtained from in Eq.(11)-(17). Given the \mathbf{W} and \mathbf{b} according to the STBP, we can use gradient descent optimization algorithms to effectively train SNNs for achieving high performance.

2.3 Derivative Approximation of the Non-differentiable Spike Activity

In the previous sections, we have presented how to obtain the gradient information based on STBP, but the issue of non-differentiable points at each spiking time is yet to be addressed. Actually, the derivative of output gate $g(u)$ is required for the STBP training of Eq.(11)-(21). Theoretically, $g(u)$ is a non-differentiable Dirac function of $\delta(u)$ which greatly challenges the effective learning of SNNs [23]. $g(u)$ has zero value everywhere except an infinity value at zero, which causes the gradient vanishing or exploding issue that disables the error propagation. One of existing method viewed the discontinuous points of the potential at spiking times as noise and claimed it is beneficial for the model robustness [23, 29], while it did not directly address the non-differentiability of the spike activity. To this end, we introduce four curves to approximate the derivative of spike activity denoted by h_1, h_2, h_3 and h_4 in Figure3.b:

$$h_1(u) = \frac{1}{a_1} \text{sign}(|u - \frac{V_{th}}{2}| < \frac{a_1}{2}), \quad (23)$$

$$h_2(u) = (\frac{\sqrt{a_2}}{2} - \frac{a_2}{4}|x - \frac{V_{th}}{2}|) \text{sign}(\frac{2}{\sqrt{a_2}} - |u - \frac{V_{th}}{2}|), \quad (24)$$

$$h_3(u) = \frac{1}{a_3} \frac{e^{\frac{V_{th}-u}{a_3}}}{(1 + e^{\frac{V_{th}-u}{a_3}})^2}, \quad (25)$$

$$h_4(u) = \frac{1}{\sqrt{2\pi a_4}} e^{-\frac{(u - \frac{V_{th}}{2})^2}{2a_4}}, \quad (26)$$

where $a_i (i = 1, 2, 3, 4)$ determines the curve shape and steep degree. In fact, h_1, h_2, h_3 and h_4 are the derivative of the rectangular function, polynomial function, sigmoid function and Gaussian

cumulative distribution function, respectively. To be consistent with the Dirac function $\delta(u)$, we introduce the coefficient a_i to ensure the integral of each function is 1. Obviously, it can be proven that all the above candidates satisfy that

$$\lim_{a_i \rightarrow 0^+} h_i(u) = \frac{dg}{du}, i = 1, 2, 3, 4. \quad (27)$$

Thus, $\frac{\partial g}{\partial u}$ in Eq.(11)-(21) for STBP can be approximated by

$$\frac{dg}{du} \approx \frac{dh_i}{du}. \quad (28)$$

In section 3.3, we will analyze the influence on the SNNs performance with different curves and different values of a_i .

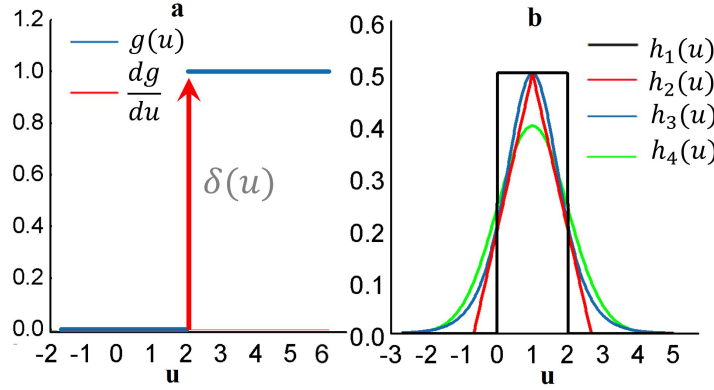


Figure 3: **Derivative approximation of the non-differentiable spike activity.** (a) Step activation function of the spike activity and its original derivative function which is a typical Dirac function $\delta(u)$ with infinite value at $u = 0$ and zero value at other points. This non-differentiable property disables the error propagation. (b) Several typical curves to approximate the derivative of spike activity.

3 Results

3.1 Parameter Initialization

The initialization of parameters, such as the weights, thresholds and other parameters, is crucial for stabilizing the firing activities of the whole network. We should simultaneously ensure timely response of pre-synaptic stimulus but avoid too much spikes that reduces the neuronal selectivity. As it is known that the multiply-accumulate operations of the pre-spikes and weights, and the threshold comparison are two key steps for the computation in the forward pass. This indicates the relative magnitude between the weights and thresholds determines the effectiveness of parameter initialization. In this paper, we fix the threshold to be constant in each neuron for simplification, and only adjust the weights to control the activity balance. Firstly, we initial all the weight parameters sampling from the standard uniform distribution

$$\mathbf{W} \sim U[-1, 1] \quad (29)$$

Then, we normalize these parameters by

$$w_{ij}^n = \frac{w_{ij}^n}{\sqrt{\sum_{j=1}^{l(n-1)} w_{ij}^n{}^2}}, \quad i = 1, \dots, l(n) \quad (30)$$

The set of other parameters is presented in Table1. Furthermore, throughout all the simulations in our work, any complex skill as in [19, 23] is no longer required, such as the fixed-amount-proportional reset, error normalization, weight/threshold regularization, etc.

Table 1: Parameters set in our experiments

Network parameter	Description	Value
T	Time window	30ms
V_{th}	Threshold (MNIST/object detection dataset/N-MNIST)	1.5, 2.0, 0.2
τ	Decay factor (MNIST/object detection dataset/N-MNIST)	0.1ms, 0.15ms, 0.2ms
a_1, a_2, a_3, a_4	Derivative approximation parameters(Figure3)	1.0
dt	Simulation time step	1ms
r	Learning rate (SGD)	0.5
$\beta_1, \beta_2, \lambda$	Adam parameters	0.9, 0.999, $1 \cdot 10^{-8}$

3.2 Dataset Experiments

We test our SNNs model and the STBP training method on various datasets, including the static MNIST and a custom object detection dataset, as well as the dynamic N-MNIST dataset. The input of the first layer should be a spike train, which requires us to convert the samples from the static datasets into spike events. To this end, the Bernoulli sampling from original pixel intensity to the spike rate is used in this paper.

3.2.1 Spatio-temporal fully connected neural network

Static Dataset. The MNIST dataset of handwritten digits [30] (figure4.b) and a custom dataset for object detection [14] (figure4.a) are chosen to test our method. MNIST is comprised of a training set with 60,000 labelled hand-written digits, and a testing set of other 10,000 labelled digits, which are generated from the postal codes of 0-9. Each digit sample is a 28×28 grayscale image. The object detection dataset is a two-category image dataset created by our lab for pedestrian detection. It includes 1509 training samples and 631 testing samples of 28×28 grayscale image. By detecting whether there is a pedestrian, an image sample is labelled by 0 or 1, as illustrated in Figure4.a. The upper and lower sub-figures in Figure4.c are the spike pattern of 25 input neurons converted from the center patch of 5×5 pixels of a sample example on the object detection dataset and MNIST, respectively. Figure4.d illustrates an example for the spike pattern of output layer within 15ms before and after the STBP training over the stimulus of digit 9. At the beginning, neurons in the output layer randomly fires, while after the training the 10th neuron coding digit 9 fires most intensively that indicates correct inference is achieved.

Table 2: Comparison with the state-of-the-art spiking networks with similar architecture on MNIST.

Model	Network structure	Training skills	Accuracy
Spiking RBM (STDP) [31]	784-500-40	None	93.16%
Spiking RBM(pre-training*) [20]	784-500-500-10	None	97.48%
Spiking MLP(pre-training*) [19]	784-1200-1200-10	Weight normalization	98.64%
Spiking MLP(BP) [22]	784-200-200-10	None	97.66%
Spiking MLP(STDP) [15]	784-6400	None	95.00%
Spiking MLP(BP) [23]	784-800-10	Error normalization/ parameter regularization	98.71%
Spiking MLP(STBP)	784-800-10	None	98.89%

We mainly compare with these methods that have the similar network architecture, and * means that their model is based on pre-trained ANN models.

Table2 compares our method with several other advanced results that use the similar MLP architecture on MNIST. Although we do not use any complex skill, the proposed STBP training method also outperforms all the reported results. We can achieve 98.89% testing accuracy only after 200 epochs which performs the best. Table3 compares our model with the typical MLP on the object detection dataset. The contrast model is one of the typical artificial neural networks (ANNs), i.e. not SNNs, and in the following we use 'non-spiking network' to distinguish them. It can be seen that our model achieves better performance than the non-spiking MLP. Note that the overall firing rate

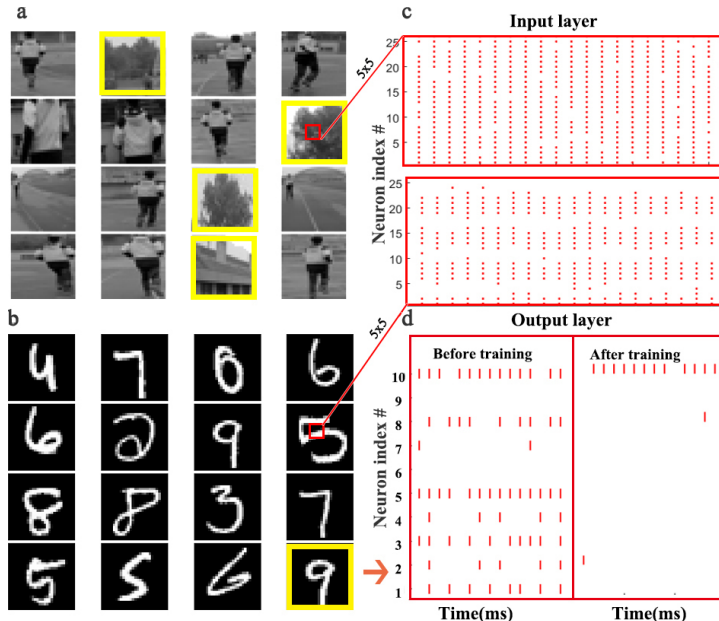


Figure 4: **Static dataset experiments.** (a) A custom dataset for object detection. This dataset is a two-category image set built by our lab for pedestrian detection. By detecting whether there is a pedestrian, an image sample is labelled by 0 or 1. The images in the yellow boxes are labelled as 1, and the rest ones are marked as 0. (b)MNIST dataset. (c) Raster plot of the spike pattern of 49 input neurons converted from the center patch of 5×5 pixels of a sample example on the object detection dataset (up) and MNIST (down). (d) Raster plot presents the comparison of output spike pattern before and after the STBP training over a digit 9 on MNIST dataset.

of the input spike train from the object detection dataset is higher than the one from MNIST dataset, so we increase its threshold to 2.0 in the simulation experiments.

Table 3: Comparison with the typical MLP over object detection dataset.

Model	Network structure	Accuracy	
		Mean	Interval*
Non-spiking MLP(BP)	784-400-10	98.31%	[97.62%, 98.57%]
Spiking MLP(STBP)	784-400-10	98.34%	[97.94%, 98.57%]

* results with epochs [201,210].

Dynamic Dataset. Compared with the static dataset, dynamic dataset, such as the N-MNIST [32], contains richer temporal features, and therefore it is more suitable to exploit SNN’s potential ability. We use the N-MNIST database as an example to evaluate the capability of our STBP method on dynamic dataset. N-MNIST converts the mentioned static MNIST dataset into its dynamic version of spike train by using the dynamic vision sensor (DVS) [33]. For each original sample from MNIST, the work [32] controls the DVS to move in the direction of three sides of the isosceles triangle in turn (figure5.b) and collects the generated spike train which is triggered by the intensity change at each pixel. Figure5.a records the saccade results on digit 0. Each sub-graph records the spike train within 10ms and each 100ms represents one saccade period. Due to the two possible change directions of each pixel intensity (brighter or darker), DVS could capture the corresponding two kinds of spike events, denoted by on-event and off-event, respectively (figure5.c). Since N-MNIST allows the relative shift of images during the saccade process, it produces 34×34 pixel range. And from the spatio-temporal representation in figure5.c, we can see that the on-events and off-events are so different that we use two channel to distinguish it. Therefore, the network structure is $34 \times 34 \times 2$ -400-400-10.

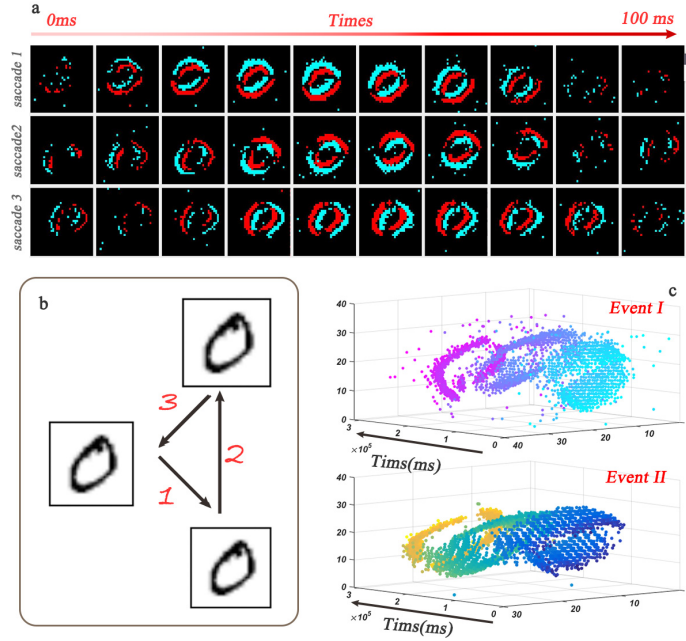


Figure 5: **Dynamic dataset of N-MNIST.** (a) Each sub-picture shows a 10ms-width spike train during the saccades. (b) Spike train is generated by moving the dynamic vision sensor (DVS) in turn towards the direction of 1, 2 and 3. (c) Spatio-temporal representation of the spike train from digit 0 [32] where the upper one and lower one denote the on-events and off-events, respectively.

Table 4: Comparison with state-of-the-art networks over N-MNIST.

Model	Network structure	Training skills	Accuracy
Non-spiking CNN(BP) [24]	-	None	95.30%
Non-spiking CNN(BP) [34]	-	None	98.30%
Non-spiking MLP(BP) [23]	784-800-10	None	97.80%
LSTM(BPTT) [24]	-	Batch normalization	97.05%
Phased-LSTM(BPTT) [24]	-	None	97.38%
Spiking CNN(pre-training*) [34]	-	None	95.72%
Spiking SNN(BP) [23]	784-800-10	Error normalization/ parameter regularization	98.74%
Spiking (BP) [35]	784-10000-10	None	92.87%
Spiking SNN(STBP)	784-400-400-10	None	98.75%

We only show the network structure based on MLP, and the other network structure refers to the above references. *means that their model is based on pre-trained ANN models.

Table4 compares our STBP method with some state-of-the-art results on N-MNIST dataset. The upper 5 results are based on ANNs, and lower 4 results including our method uses SNNs. The ANNs methods usually adopt a frame-based method, which collects the spike events in a time interval ($50ms \sim 300ms$) to form a frame of image, and use the conventional algorithms for image classification to train the networks. Since the transformed images are often blurred, the frame-based preprocessing is harmful for model performance and abandons the hardware friendly event-driven paradigm. As can be seen from Table4, the models of ANN are generally worsen than the models of SNNs. In contrast, SNNs could naturally handle event stream patterns, and by better use of spatio-temporal feature of event streams, our proposed STBP method achieves best accuracy of 98.75% when compared all the reported ANNs and SNNs methods. The greatest advantage of our method is that we did not use any complex training skills, which is beneficial for future hardware implementation.

3.2.2 Spatio-temporal convolution neural network

Extending our framework to convolution neural network structure allows the network going deeper and grants network more powerful SD information. Here we use our framework to establish the spatio-temporal convolution neural network. Compared with our spatio-temporal fully connected network, the main difference is the processing of the input image, where we use the convolution in place of the weighted summation. Specifically, in the convolution layer, each convolution neuron receives the convoluted input and updates its state according to the LIF model. In the pooling layer, because the binary coding of SNNs is inappropriate for standard max pooling, we use the average pooling instead.

Table 5: Comparison with other spiking CNN over MNIST.

Model	Network structure	Accuracy
Spiking CNN (pre-training*) [13]	$28 \times 28 \times 1-12C5-P2-64C5-P2-10$	99.12%
Spiking CNN(BP) [23]	$28 \times 28 \times 1-20C5-P2-50C5-P2-200-10$	99.31%
Spiking CNN (STBP)	$28 \times 28 \times 1-15C5-P2-40C5-P2-300-10$	99.42%

We mainly compare with these methods that have the similar network architecture, and * means that their model is based on pre-trained ANN models.

Table 6: Comparison with the typical CNN over object detection dataset.

Model	Network structure	Accuracy	
		Mean	Interval*
Non-spiking CNN(BP)	$28 \times 28 \times 1-6C3-300-10$	98.57%	[98.57%, 98.57%]
Spiking CNN(STBP)	$28 \times 28 \times 1-6C3-300-10$	98.59%	[98.26%, 98.89%]

* results with epochs [201,210].

Our spiking CNN model are also tested on the MNIST dataset as well as the object detection dataset . In the MNIST, our network contains one convolution layers with kernel size of 5×5 and two average pooling layers alternatively, followed by one hidden layer. And like traditional CNN, we use the elastic distortion [36] to preprocess dataset. Table5 records the state-of-the-art performance spiking convolution neural networks over MNIST dataset. Our proposed spiking CNN model obtain 98.42% accuracy, which outperforms other reported spiking networks with slightly lighter structure. Furthermore, we configure the same network structure on a custom object detection database to evaluate the proposed model performance. The testing accuracy is reported after training 200 epochs. Table6 indicates our spiking CNN model could achieve a competitive performance with the non-spiking CNN.

3.3 Performance Analysis

3.3.1 The Impact of Derivative Approximation Curves

In section 2.2, we introduce different curves to approximate the ideal derivative of the spike activity. Here we try to analyze the influence of different approximation curves on the testing accuracy. The experiments are also conducted on the MNIST dataset, and the network structure is $784 - 400 - 10$. The testing accuracy is reported after training 200 epochs. Firstly, we compare the impact of different curve shapes on model performance. In our simulation we use the mentioned h_1, h_2, h_3 and h_4 shown in Figure3.b. Figure6.a illustrates the results of approximations of different shapes. We observe that different nonlinear curves, such as h_1, h_2, h_3 and h_4 , only present small variations on the performance.

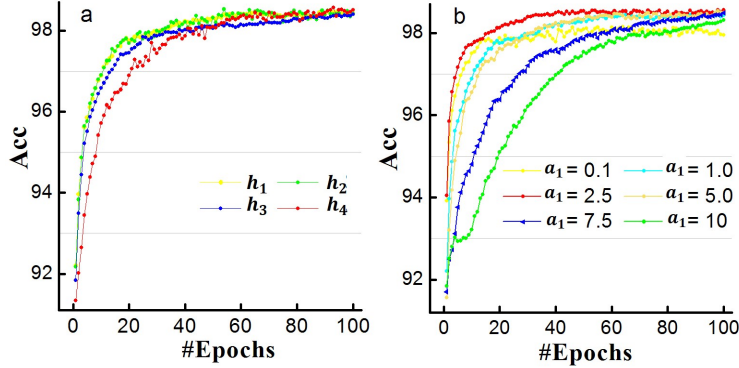


Figure 6: **Comparisons of different derivation approximation curves.** (a) The impact of different approximations. (b) The impact of different widths of regular approximation.

Furthermore, we use the rectangular approximation as an example to explore the impact of width on the experiment results. We set $a_1 = 0.1, 1.0, 2.5, 5.0, 7.5, 10$ and corresponding results are plotted in figure6.b. Different colors denote different a_1 values. Both too large and too small a_1 value would cause worse performance and in our simulation, $a_1 = 2.5$ achieves the highest testing accuracy, which implies the width of rectangle influences the model performance. Combining figure 6.a and figure 6.b, it indicates that the key point for approximating the derivation of the spike activity is to capture the nonlinear nature, while the specific shape is not so critical.

3.3.2 The Impact of Temporal Domain

A major contribution of this work is introducing the temporal domain (TD) into the existing spatial domain (SD) based BP training method, which makes full use of the spatio-temporal dynamics of SNNs and enables the high-performance training. Now we quantitatively analyze the impact of the TD item. The experiment configurations keep the same with the previous section ($784 - 400 - 10$) and we also report the testing results after training 200 epochs. Here the existing BP in the SD is termed as SDBP.

Table7 records the simulation results. The testing accuracy of SDBP is lower than the accuracy of the STBP on different dataset, which shows the time information is beneficial for model performance. Specifically, the SDBP has a 1.21% loss of accuracy on the objective tracking dataset, which is 5 times larger than the loss on the MNIST. And results also imply that the performance of SDBP is not stable enough. In addition to the interference of the dataset itself, the reason for this variation may be the instability of SNNs training. Actually, the training of SNNs relies heavily on the parameter initialization, which is also a great challenge for SNNs applications. In many reported works, researchers usually leverage some special skills or mechanisms to improve the training performance, such as the lateral inhibition, regularization, normalization, etc. In contrast, by using our STBP

Table 7: Comparison for the SDBP model and the STBP model on different datasets.

Model	Dataset	Network structure	Training skills	Accuracy	
				Mean	Interval*
Spiking MLP (SDBP)	Objective tracking	784-400-10	None	97.11%	[96.04%,97.78%]
	MNIST	784-400-10	None	98.29%	[98.23%, 98.39%]
Spiking MLP (STBP)	Objective tracking	784-400-10	None	98.32%	[97.94%, 98.57%]
	MNIST	784-400-10	None	98.48%	[98.42%, 98.51%]

* results with epochs [201,210].

training method, much higher performance can be achieved on the same network. Specifically, the testing accuracy of STBP reaches 98.48% on MNIST and 98.32% on the object detection dataset. Note that the STBP can achieve high accuracy without using any complex training skills. This stability and robustness indicate that the dynamics in the TD fundamentally includes great potential for the SNNs computing and this work indeed provides a new idea.

4 Conclusion and Discussion

In this work, a unified framework that allows supervised training spiking neural networks (SNNs) just like implementing backpropagation in deep neural networks (DNNs) has been built by exploiting the spatio-temporal information in the networks. Our major contributions are summarized as follows:

1. We have presented a framework based on an iterative leaky integrate-and-fire (LIF) model, which enables us to implement spatio-temporal backpropagation (STBP) on SNNs. Unlike previous methods primarily focused on its spatial domain features, our framework further combines and exploits the features of SNNs in both the spatial domain and temporal domain;
2. We have designed the STBP training algorithm and implemented it on both MLP and CNN architectures. The STBP has been verified on both static and dynamic datasets. Results have shown that our model is superior to the state-of-the-art SNNs, and outperforms DNNs with the same network size on dynamic N-MNIST dataset. An attractive advantage of our algorithm is that it doesn't need extra training techniques which generally required by existing schemes, and is easier to be implemented in large-scale networks. Results also have revealed that the use of spatio-temporal complexity to solve problems could fulfill the potential of SNNs better;
3. We have introduced an approximated derivative to address the non-differentiable issue of the spike activity. Controlled experiment indicates that the width of rectangle would affect the model's performance and the key point for approximations is to capture the nonlinear nature, while the specific shape is not so critical.

Because the brain combines complexity in the temporal and spatial domains to handle input information, we also would like to claim that implementing STBP on SNNs is more bio-plausible than applying BP on DNNs. The property of STBP that doesn't rely on too many training skills makes it more hardware-friendly and useful for the design of neuromorphic chip with online learning ability. Regarding the future research topics, two issues we believe are quite necessary and very important. One is to apply our framework to tackle more problems with the timing characteristics, such as dynamic data processing, video stream identification and speech recognition. The other is how to accelerate the supervised training of large scale SNNs based on GPUs/CPUs or neuromorphic chips. The former aims to further exploit the rich spatio-temporal features of SNNs to deal with dynamic problems, and the later may greatly prompt the applications of large scale of SNNs in real life scenarios.

References

- [1] Poonam Chaudhari and Himanshu Agarwal. *Progressive Review Towards Deep Learning Techniques*. Springer Singapore, 2017.
- [2] Li Deng and Dong Yu. Deep learning: Methods and applications. *Foundations and Trends in Signal Processing*, 7(3):197–387, 2014.
- [3] Jia, Yangqing, Shelhamer, Evan, Donahue, Jeff, Karayev, Sergey, Long, and Jonathan. Caffe: Convolutional architecture for fast feature embedding. *Eprint Arxiv*, pages 675–678, 2014.
- [4] Geoffrey Hinton, Li Deng, Dong Yu, and George E. Dahl. Deep neural networks for acoustic modeling in speech recognition: The shared views of four research groups. *IEEE Signal Processing Magazine*, 29(6):82–97, 2012.
- [5] Kaiming He, Xiangyu Zhang, Shaoqing Ren, and Jian Sun. *Spatial Pyramid Pooling in Deep Convolutional Networks for Visual Recognition*. Springer International Publishing, 2014.
- [6] Xu Zhang, Ziyi Xu, Craig Henriquez, and Silvia Ferrari. Spike-based indirect training of a spiking neural network-controlled virtual insect. In *Decision and Control (CDC), 2013 IEEE 52nd Annual Conference on*, pages 6798–6805. IEEE, 2013.
- [7] Jacob N. Allen, Hoda S. Abdel-Aty-Zohdy, and Robert L. Ewing. Cognitive processing using spiking neural networks. In *IEEE 2009 National Aerospace and Electronics Conference*, pages 56–64, 2009.
- [8] Nikola Kasabov and Elisa Capecchi. Spiking neural network methodology for modelling, classification and understanding of eeg spatio-temporal data measuring cognitive processes. *Information Sciences*, 294(C):565–575, 2015.
- [9] Ben Varkey Benjamin, Peiran Gao, Emmett Mcquinn, Swadesh Choudhary, Anand R. Chandrasekaran, Jean Marie Bussat, Rodrigo Alvarez-Icaza, John V. Arthur, Paul A. Merolla, and Kwabena Boahen. Neurogrid: A mixed-analog-digital multichip system for large-scale neural simulations. *Proceedings of the IEEE*, 102(5):699–716, 2014.
- [10] P. A. Merolla, J. V. Arthur, R Alvarezicaza, A. S. Cassidy, J Sawada, F Akopyan, B. L. Jackson, N Imam, C. Guo, and Y Nakamura. Artificial brains. a million spiking-neuron integrated circuit with a scalable communication network and interface. *Science*, 345(6197):668–73, 2014.
- [11] Steve B Furber, Francesco Galluppi, Steve Temple, and Luis A Plana. The spinnaker project. *Proceedings of the IEEE*, 102(5):652–665, 2014.
- [12] Tiffany Hwu, Jacob Isbell, Nicolas Oros, and Jeffrey Krichmar. A self-driving robot using deep convolutional neural networks on neuromorphic hardware. *arXiv.org*, 2016.
- [13] S. K. Esser, P. A. Merolla, J. V. Arthur, A. S. Cassidy, R Appuswamy, A Andreopoulos, D. J. Berg, J. L. McKinstry, T Melano, and D. R. Barch. Convolutional networks for fast, energy-efficient neuromorphic computing. *Proceedings of the National Academy of Sciences of the United States of America*, 113(41):11441, 2016.
- [14] S. Song Zhang, L.P. Shi. Creating more intelligent robots through brain-inspired computing. *Science(suppl)*, 354, 2016.
- [15] Peter U. Diehl and Matthew Cook. Unsupervised learning of digit recognition using spike-timing-dependent plasticity. *Frontiers in Computational Neuroscience*, 9:99, 2015.
- [16] Damien Querlioz, Olivier Bichler, Philippe Dollfus, and Christian Gamrat. Immunity to device variations in a spiking neural network with memristive nanodevices. *IEEE Transactions on Nanotechnology*, 12(3):288–295, 2013.
- [17] Saeed Reza Kheradpisheh, Mohammad Ganjtabesh, and Timothee Masquelier. Bio-inspired unsupervised learning of visual features leads to robust invariant object recognition. *Neurocomputing*, 205(C):382–392, 2016.
- [18] J. A. Perezcarrasco, B. Zhao, C Serrano, B Acha, T Serranogotarredona, S. Chen, and B Linaresbarranco. Mapping from frame-driven to frame-free event-driven vision systems by low-rate rate-coding and coincidence processing. application to feed forward convnets. *IEEE Transactions on Pattern Analysis and Machine Intelligence*, 35(11):2706–19, 2013.

- [19] P. U Diehl, D Neil, J Binas, and M Cook. Fast-classifying, high-accuracy spiking deep networks through weight and threshold balancing. In *International Joint Conference on Neural Networks*, pages 1–8, 2015.
- [20] O’Connor Peter, Neil Daniel, Shih Chii Liu, Delbruck Tobi, and Pfeiffer Michael. Real-time classification and sensor fusion with a spiking deep belief network. *Frontiers in Neuroscience*, 7:178, 2013.
- [21] Eric Hunsberger and Chris Eliasmith. Spiking deep networks with lif neurons. *Computer Science*, 2015.
- [22] Peter O’Connor and Max Welling. Deep spiking networks. *arXiv.org*, 2016.
- [23] J. H. Lee, T Delbruck, and M Pfeiffer. Training deep spiking neural networks using backpropagation. *Frontiers in Neuroscience*, 10, 2016.
- [24] Daniel Neil, Michael Pfeiffer, and Shih Chii Liu. Phased lstm: Accelerating recurrent network training for long or event-based sequences. *arXiv.org*, 2016.
- [25] F. A. Gers, J Schmidhuber, and F Cummins. Learning to forget: continual prediction with lstm. *Neural Computation*, 12(10):2451, 1999.
- [26] Sepp Hochreiter and Jürgen Schmidhuber. Long short-term memory. *Neural computation*, 9(8):1735–1780, 1997.
- [27] Junyoung Chung, Caglar Gulcehre, Kyunghyun Cho, and Yoshua Bengio. Gated feedback recurrent neural networks. *Computer Science*, pages 2067–2075, 2015.
- [28] Paul J Werbos. Backpropagation through time: what it does and how to do it. *Proceedings of the IEEE*, 78(10):1550–1560, 1990.
- [29] Yoshua Bengio, Thomas Mesnard, Asja Fischer, Saizheng Zhang, and Yuhai Wu. An objective function for stdp. *Computer Science*, 2015.
- [30] Yann Lecun, Leon Bottou, Yoshua Bengio, and Patrick Haffner. Gradient-based learning applied to document recognition. *Proceedings of the IEEE*, 86(11):2278–2324, 1998.
- [31] E Neftci, S Das, B Pedroni, K Kreutzdelgado, and G Cauwenberghs. Event-driven contrastive divergence for spiking neuromorphic systems. *Frontiers in Neuroscience*, 7:272, 2013.
- [32] G Orchard, A Jayawant, G. K. Cohen, and N Thakor. Converting static image datasets to spiking neuromorphic datasets using saccades. *Frontiers in Neuroscience*, 9, 2015.
- [33] P. Lichtsteiner, C. Posch, and T. Delbruck. A 128x128 120db 15us latency asynchronous temporal contrast vision sensor. *IEEE Journal of Solid-State Circuits*, 43(2):566–576, 2007.
- [34] Daniel Neil and Shih Chii Liu. Effective sensor fusion with event-based sensors and deep network architectures. In *IEEE Int. Symposium on Circuits and Systems*, 2016.
- [35] Gregory K. Cohen, Garrick Orchard, Sio Hoi Leng, Jonathan Tapson, Ryad B. Benosman, and Andre Van Schaik. Skimming digits: Neuromorphic classification of spike-encoded images. *Frontiers in Neuroscience*, 10(184), 2016.
- [36] Patrice Y. Simard, Dave Steinkraus, and John C. Platt. Best practices for convolutional neural networks applied to visual document analysis. In *International Conference on Document Analysis and Recognition*, page 958, 2003.